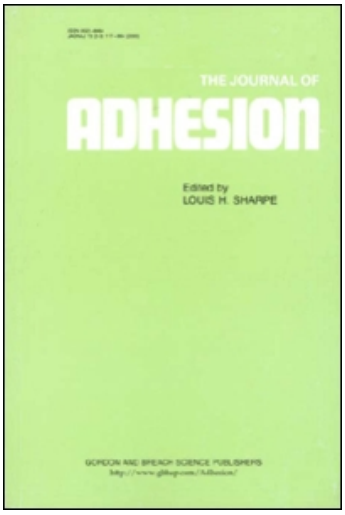

The Journal of Adhesion
Publication details, including instructions for authors and subscription information:
http://www.informaworld.com/smpp/title~content=t713453635

Effect of Piezoelectric Patches on the Behavior of Adhesively Bonded Single Lap Joints

S. M. R. Khalili[ab]; R. Eslami Farsani[c]; A. Khoeini[a]
[a] Department of Mechanical Engineering, South Tehran Branch, Islamic Azad University, Tehran, Iran [b] Faculty of Engineering, Kingston University, London, UK [c] Centre of Excellence for Research in Advanced Materials and Structures, Faculty of Mechanical Engineering, K.N. Toosi University of Technology, Tehran, Iran

Online publication date: 10 June 2010

To cite this Article Khalili, S. M. R. , Farsani, R. Eslami and Khoeini, A.(2010) 'Effect of Piezoelectric Patches on the Behavior of Adhesively Bonded Single Lap Joints', The Journal of Adhesion, 86: 5, 601 — 629
To link to this Article: DOI: 10.1080/00218464.2010.484315
URL: http://dx.doi.org/10.1080/00218464.2010.484315

The Journal of Adhesion, 86:601–629, 2010

ISSN: 0021-8464 print/1545-5823 online
DOI: 10.1080/00218464.2010.484315

Taylor & Francis
Taylor & Francis Group

Effect of Piezoelectric Patches on the Behavior of Adhesively Bonded Single Lap Joints

S. M. R. Khalili[1,3], R. Eslami Farsani[2], and A. Khoeini[1]
[1]Department of Mechanical Engineering, South Tehran Branch, Islamic Azad University, Tehran, Iran
[2]Centre of Excellence for Research in Advanced Materials and Structures, Faculty of Mechanical Engineering, K.N. Toosi University of Technology, Tehran, Iran
[3]Faculty of Engineering, Kingston University, London, UK

In order to reduce the influence of the maximum peel and shear stress concentrations in the adhesive layer, a smart adhesively bonded single lap joint system was developed by surface bonding of piezoelectric patches onto a typical single lap joint. The forces and bending moments at the edges of the developed smart joint system can be adaptively controlled by adjusting the applied electric field in the piezoelectric patches, thus reducing the peel and shear stresses concentration effect in the adhesive layer. In order to verify the effect of surface bonding of piezoelectric patches in smart single lap adhesive joints, an analytical model based on shear lag assumptions was developed to evaluate the shear stress distribution and to predict the peel stress. For this purpose, the beam on elastic foundation (BOEF) approach in the adhesive layer was used. It was established that the piezoelectric patched joint could reduce the stress concentrations in the lap joint edges. The influence of electric field, location, and size of the piezoelectric patches in the single lap joint was also investigated.

Keywords: Adhesive joints; Patch; Piezoelectric; Single lap; Stress analysis

Received 22 June 2009; in final form 18 February 2010.
Presented in part at the 3rd International Conference on Advanced Computational Engineering and Experimenting (ACE-X 2009), Rome, Italy, 22–23 June 2009.
Address correspondence to S. M. R. Khalili, Centre of Excellence for Research in Advanced Materials and Structures, Faculty of Mechanical Engineering, K.N. Toosi University of Technology, Tehran, Iran. E-mail: smrkhalili2005@gmail.com

1. INTRODUCTION

Adhesively bonded joints are essential in the manufacturing and repair of spacecraft, aircraft, and automotive structures due to their ability to join dissimilar materials. Adhesive bonding is advantageous, because the distribution of stresses over a bonded region is less critical than in other fastening techniques. Also, one can notice an improved appearance of the products, good sealing, low stress concentration, and fatigue resistance [1]. More recent stress analysis methods are based on theoretical elasticity formulation or the finite element method (FEM). One of the earliest works cited in the literatures is the work of Goland and Reissner [2]. They assumed the adhesive layer to be a relatively flexible layer, and obtained a two-dimensional, elasticity-based analytical solution for assessing the stress distribution in a lap joint. Adams *et al.* [3] obtained theoretical stress distributions from a two-dimensional finite element idealization in adhesively bonded lap, bevel, and scarf joints between adherends of high tensile strength carbon fibre reinforced plastic.

In order to reduce the effect of stress concentration in a joint, some works were carried out theoretically to demonstrate that the stress distribution in an adhesive layer could be reoriented by adjusting the adherends thickness, length, and material properties [4–6]. Researchers have also developed other practical solutions to reduce concentrations of the shear and peel stresses, by rounding off sharp edges, spew fillets, and tapering of the adherends [4,5]. In a more recent work, Khalili *et al.* [7] investigated numerically the change in the joint strength by reinforcing the adhesive region in a single lap joint by fibres. They concluded that reinforcing the adhesive region resulted in increasing the bond strength of the lap joint. Also, da Silva and Adams [8] proposed a technique to reduce the peel stresses in the composite and to increase the joint strength at low temperatures by using an internal taper and adhesive fillet arrangement, provided the adhesive has a high tensile strength and the thermal stresses are not important.

Obviously, those previous improved methods are traditionally focused on the mechanical stiffening methods, as mentioned above. Recently, Cheng and Taheri [9,10] introduced a smart adhesively bonded joint concept to the traditional adhesively bonded joint by partially integrating piezoelectric ceramic patches as actuators, and reducing the stress concentration in the adhesive joint system. They analyzed the peel and shear stresses in the adhesive layer on the basis of the first-order shear deformation theory (FOST).

More recently, Lee and Kim [11] investigated the symmetric single lap joint with elastic-perfectly plastic adhesive by an analytical model

based on shear lag and beam on elastic foundation (BOEF) models. The model could accurately predict shear stress to within 1% and peel stress to within 13% for an elastic-perfectly plastic adhesive.

In the present work, to analyse the effect of surface bonding of piezoelectric patches in smart single lap adhesive joint, an analytical model based on the shear lag assumption was developed to evaluate the shear stress distribution and the BOEF approach in the adhesive layer was used to predict the peel stress. The joint was considered to be a symmetric single lap and the behavior was elastic. The joint was loaded by in-plane axial tension forces and governing equations were solved directly using the linear constitutive relationship of the adhesive. In order to check the validity of the results, they were compared with those reported in [9]. The effect of electric field, size, and location of piezoelectric patches on the peel and shear stress distributions was investigated.

2. SMART SINGLE LAP JOINT UNDER THE ACTION OF COMBINED MECHANICAL AND ELECTRIC LOADS

A smart single lap adhesive joint was developed by surface bonding of piezoelectric patches onto a typical single lap joint, as shown in Fig. 1. The forces and bending moments at the edges of the developed smart joint system can be adaptively controlled by adjusting the applied electric field in the piezoelectric patches, thus reducing the influence of the peel and shear stresses concentration in the adhesive layer.

According to the work of Roberts [5] on the influence of joint-edge loads on the stress concentration, the peel and shear stresses of a

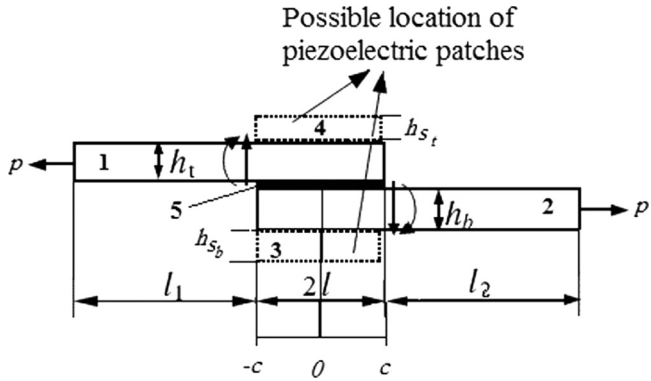

FIGURE 1 Developed smart adhesive bonded single lap joint. 1, 2–Adherends; 3, 4–Piezoelectric patches; 5–Adhesive.

single lap joint are distributed symmetrically and their peak values at the joint edges can be reduced by varying the applied load.

By considering the proposed smart single lap joint subjected to an axial tension force, as shown in Fig. 1, it is assumed that the plane section in each adherend remains plane to carry the applied force and bending moment. By considering the representative segment model as shown in Fig. 2 and the coordinate system used in Fig. 3, the equilibrium equations for different parts of the smart single lap joint can be derived on the basis of assumptions of the classical plate theory as follows [9]:

$$
\begin{aligned}
D_{11}\frac{\partial^4 w_1}{\partial x_1^4} - p\frac{\partial^2 w_1}{\partial x_1^2} &= 0 \quad 0 \le x_1 \le l_1,\\
D_{12}\frac{\partial^4 w_2}{\partial x_2^4} - p\frac{\partial^2 w_2}{\partial x_2^2} &= 0 \quad 0 \le x_2 \le l_3,\\
D_{123}\frac{\partial^4 w_3}{\partial x_3^4} + \frac{\partial^2 M_{p^3}(x_3)}{\partial x_3^2} - (p + N^0_{p^3})\frac{\partial^2 w_3}{\partial x_3^2} &= 0 \quad 0 \le x_3 \le l_4\\
D_{12}\frac{\partial^4 w_4}{\partial x_4^4} - p\frac{\partial^2 w_4}{\partial x_4^2} &= 0 \quad 0 \le x_4 \le l_5,\\
D_{124}\frac{\partial^4 w_5}{\partial x_5^4} + \frac{\partial^2 M_{p^4}(x_5)}{\partial x_5^2} - (p + N^0_{p^4})\frac{\partial^2 w_5}{\partial x_5^2} &= 0 \quad 0 \le x_5 \le l_6,\\
D_{12}\frac{\partial^4 w_6}{\partial x_6^4} - p\frac{\partial^2 w_6}{\partial x_6^2} &= 0 \quad 0 \le x_6 \le l_7,\\
D_{22}\frac{\partial^4 w_7}{\partial x_7^4} - p\frac{\partial^2 w_7}{\partial x_7^2} &= 0 \quad 0 \le x_7 \le l_2,
\end{aligned}
\tag{1}
$$

where D_{11}, D_{22}, D_{123}, D_{124}, and D_{12} represent the flexural rigidities of different segments of the smart joint respectively, as shown in Fig. 3

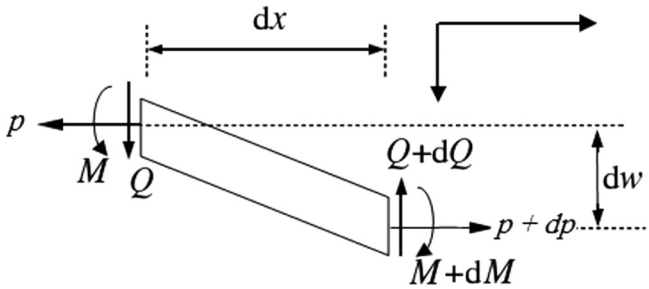

FIGURE 2 A representative segment model of a beam subjected to combined bending and axial forces.

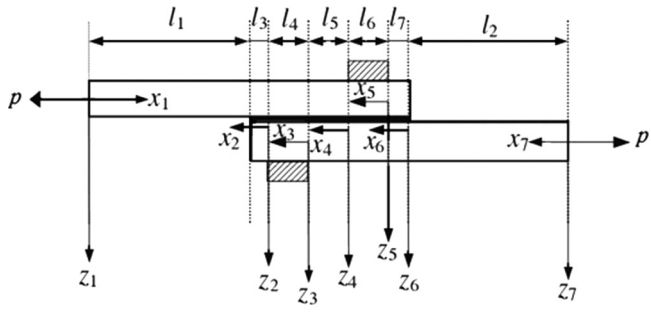

FIGURE 3 Coordinate system of the smart single lap joint with anti-symmetric surface bonded piezoelectric patches defined in Ref. [9].

and defined in [9]. p is the in-plane axial tension force applied to the joint. Moreover d_{12}, d_{123}, and d_{124} are the neutral planes eccentric distance of the different parts of the smart joint, and N_{p_i} and M_{p_i} $(i = 3, 4)$ denote the resultant forces and moments induced by the electric field applied to the ith surface bonded piezoelectric patches [9]:

$$N_{pi} = -\int_{z_k}^{z_{k+1}} e^*_{31k} E_3 dz \quad M_{pi} = -\int_{z_k}^{z_{k+1}} e^*_{31k} E_3 z dz, \tag{2}$$

where e^*_{ijk} is the equivalent strain defined by the ratio of dielectric permittivity to piezoelectric strain coefficient. Further, the joint end boundary conditions of the smart single lap joint system can be represented by:

$$w_1 = w_{1,xx} = 0 \quad \text{at } x_1 = 0$$
$$w_7 = w_{7,xx} = 0 \quad \text{at } x_7 = 0$$

and the continuity conditions between the different parts must be satisfied as follows:

1. At the boundary $x_1 = l_1$ and $x_2 = l_3$:

$$w_1 = w_2; \quad w_{1,x} = -w_{2,x}; \quad D_{11} w_{1,xx} = D_{12} w_{2,xx} + p(h_1/2 - d_{12});$$
$$D_{11} w_{1,xxx} - p w_{1,x} = -[D_{12} w_{2,xxx} - p w_{2,x}];$$

2. At the boundary $x_2 = 0$ and $x_3 = l_4$:

$$w_2 = w_3; \quad w_{2,x} = w_{3,x}; \quad D_{12} w_{2,xx} = D_{123} w_{3,xx} + M_{p^3}(x) + p(d_{12} - d_{123});$$
$$D_{12} w_{2,xxx} - p w_{2,x} = -\left[D_{123} w_{3,xxx} + \frac{\partial M_{p^3}(x)}{\partial x} - (p + N_{p^3}) w_{3,x}\right];$$

3. At the boundary $x_3 = 0$ and $x_4 = l_5$:

$$w_3 = w_4; \quad w_{3,x} = w_{4,x}; \quad D_{123}w_{3,xx} + M_{p^3}(x_3) + p(d_{12} - d_{123}) = D_{12}w_{4,xx};$$
$$D_{123}w_{3,xxx} + \frac{\partial M_{p^3}(x)}{\partial x} - (p + N_{p^3})w_{3,x} = -(D_{12}w_{4,xxx} - pw_{4,x});$$

4. At the boundary $x_4 = 0$ and $x_5 = l_6$:

$$w_4 = w_5; \quad w_{4,x} = w_{5,x}; \quad D_{12}w_{4,xx} + p(d_{124} - d_{12}) = D_{124}w_{5,xx} + M_{p^4}(x);$$
$$D_{12}w_{4,xxx} - pw_{4,x} = -\left[D_{124}w_{5,xxx} + \frac{\partial M_{p^4}(x)}{\partial x} - (p + N_{p^4})w_{5,x}\right];$$

5. At the boundary $x_5 = 0$ and $x_6 = l_7$:

$$w_5 = w_6; \quad w_{5,x} = w_{6,x}; \quad D_{124}w_{5,xx} + M_{p^4}(x) = D_{12}w_{6,xx} + p(d_{124} - d_{12});$$
$$D_{124}w_{5,xxx} + \frac{\partial M_{p^4}(x)}{\partial x} - (p + N_{p^4})w_{5,x} = -(D_{12}w_{6,xxx} - pw_{6,x});$$

6. At the boundary $x_6 = 0$ and $x_7 = l_2$:

$$w_6 = w_7; \quad w_{6,x} = w_{7,x}; \quad D_{12}w_{6,xx} = D_{12}w_{7,xx} + p(h_2/2 - d_{12});$$
$$D_{124}w_{6,xxx} - pw_{6,x} = -[D_{22}w_{7,xxx} - pw_{7,x}];$$

where w_i, is the corresponding derivatives of the deflection, w, in each "i" segment w.r.t. the x coordinate.

Obviously, for the governing fourth-order differential equation, Eq. (1), the general analytical solution can be carried out in the following parts [9]:

For the elastic parts—

$$w_i(x_i) = A_i + B_i x_i + C_i \sinh[\alpha_i x_i] + D_i \cosh[\alpha_i x_i] \quad (i = 1, 2, 4, 6, 7) \quad (3a)$$

For the electro-elastic parts—

$$w_i(x_i) = A_i + B_i x_i + C_i \sinh[\alpha_i x_i] + D_i \cosh[\alpha_i x_i] + w_i^*(x_i) \quad (i = 3, 5) \quad (3b)$$

where A_i, B_i, C_i, and D_i are unknown constant coefficients, determined by the boundary conditions. The variable $w_i^*(x_i)$ denotes the specified solution due to the piezoelectric coupling effect and is selected based on the relative governing equations.

After substituting the general analytical solution, Eq. (3), into the relevant boundary conditions, the coefficients A_i, B_i, C_i, and D_i can be calculated and then the joint-edge applied moments M_1 and M_2

and the shearing forces Q_1 and Q_2 in the smart single lap joint can be obtained by [9]:

$$M_1 = -D_{11}\left.\frac{\partial^2 w_1}{\partial x_1^2}\right|_{x_1=l_1}; \quad M_2 = D_{22}\left.\frac{\partial^2 w_7}{\partial x_7^2}\right|_{x_7=l_2};$$
$$Q_1 = (D_{11}w_{1,xxx} - pw_{1,x})|_{x_1=l_1}; \quad Q_2 = (D_{22}w_{7,xxx} - pw_{7,x})|_{x_7=l_2}. \tag{4}$$

3. MODEL DESCRIPTION

In this section, the shear stress in the adhesive layer on the basis of the shear lag assumption and the adhesive peel stress on the basis of the beam on elastic foundation (BOEF) approach were obtained analytically. The function of the piezoelectric patch is only to supply the additional required force and moment. The piezoelectric layer was assumed to be relatively thin in comparison with the adherends. Therefore, the stiffness contribution from the piezoelectric patches is relatively small, and may be neglected when analyzing the stress distribution in the adhesive layer. Here, it is assumed that the piezoelectric patches cover the entire joint surface. Therefore, based on the above assumption, the stiffness of the adhesive layer between the piezoelectric layer and the adherends can be assumed to be negligible, while analyzing the stress distribution in the adhesive layer [9].

The adhesively bonded symmetric single lap joint with the surface bonded piezoelectric patches and all relevant geometric parameters is shown in Figs. 1 and 3. The only externally applied mechanical load is p. The following assumptions are made for the symmetric single lap joint:

1. The analysis is based on plane strain conditions;
2. Constant thickness is considered for adherends and adhesive;
3. The distributions of the shear and peel stresses are uniform through the adhesive thickness (z-direction);
4. Deformation of adherends due to transverse shear is neglected;
5. The behavior of adherends and adhesive is considered to be linear elastic;
6. The adhesively single lap joint is symmetric and the adherends are identical in thickness and material.

3.1. Governing Equations

A differential small element, dx, of the joint at any location x is shown in Fig. 4. The x-direction and z-direction displacements at the interfaces of the adherends and the adhesive, *i.e.*, at $z_1 = 0$ and

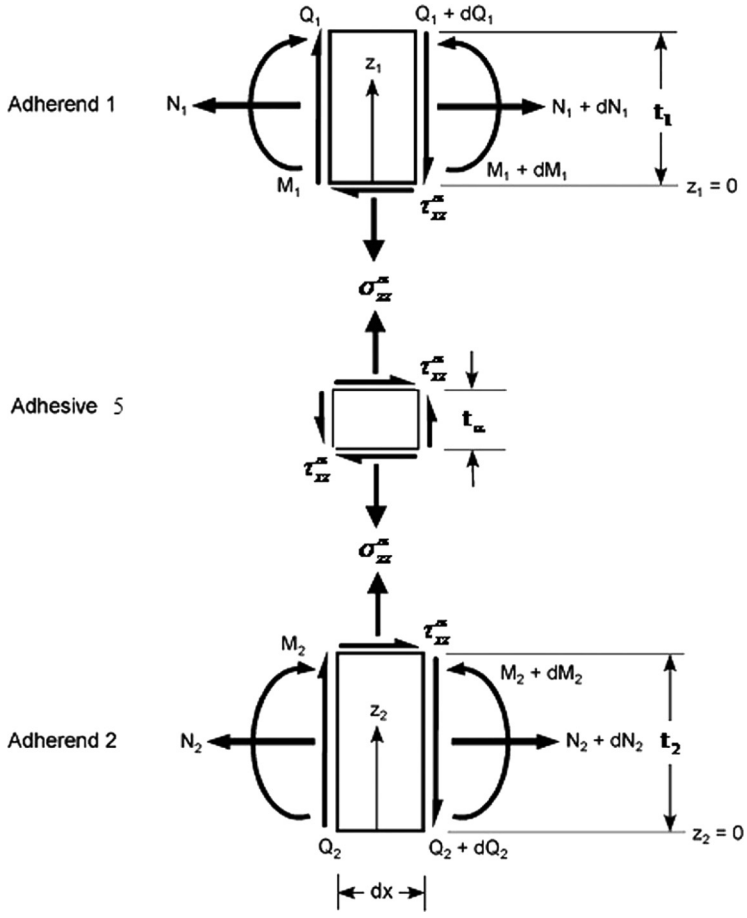

FIGURE 4 Stresses and forces on the differential small element of the joint system.

$z_2 = t_2$ are defined as u_1, w_1 and u_2, w_2, respectively. These interfacial adhesive-adherends displacements are functions of in-plane axial force resultants (N_1 and N_2), internal moment resultants (M_1 and M_2), and joint geometry and material parameters (thickness t, modulus E, and bending rigidity, D) of the adherends.

The adhesive shear strain, γ_{xz}^{α}, is determined from the interface adjacent horizontal displacements, u_1 and u_2, and the thickness, t_α, of the adhesive [11]:

$$\gamma_{xz}^{\alpha} = \frac{1}{t_\alpha}(u_1 - u_2). \tag{5}$$

Differentiating Eq. (5) with respect to x, yields:

$$\frac{d\gamma_{xz}^{\alpha}}{dx} = \frac{1}{t_{\alpha}}(\varepsilon_{x1} - \varepsilon_{x2}), \tag{6}$$

where ε_{x1} and ε_{x2} are the normal strains in the x-direction in the adherends at the adhesive interface. These quantities can be computed from the in-plane axial force resultants (N_1 and N_2) and the internal moment resultants (M_1 and M_2) based on simple beam theory. Again, differentiating Eq. (6) with respect to x yields the following relationship:

$$\begin{aligned}\frac{d^2\gamma_{xz}^{\alpha}}{dx^2} = \frac{1}{t_{\alpha}}\left[\left(\frac{1}{E_1 t_1} + \frac{1}{E_2 t_2}\right) + \frac{1}{4}\left(\frac{t_1^2}{D_1} + \frac{t_2^2}{D_2}\right)\right]\tau_{xz}^{\alpha} \\ + \frac{1}{2t_{\alpha}}\left(\frac{t_1}{D_1}Q_1 + \frac{t_2}{D_2}Q_2\right),\end{aligned} \tag{7}$$

where τ_{xy}^{α} is the adhesive shear stress and is related to N_i, M_i, and Q_i *via* force and moment equilibrium applied to the differential elements shown in Fig. 4 [11]. Also, E_i and D_i in Eq. (7) are the elastic modulus and bending rigidity of the adherends, respectively. The subscript i indicates adherends 1 and 2. The sum of the transverse shear force resultants within the adherends (Q_1 and Q_2) is zero when the joint is geometrically and materially symmetric [12]. For symmetric joints with $t_1 = t_2$, $E_1 = E_2$, and $D_1 = D_2$, Eq. (7) simplifies to the following [11]:

$$\frac{d^2\gamma_{xz}^{\alpha}}{dx^2} = \frac{1}{t_{\alpha}}\left[\frac{2}{E_1 t_1} + \frac{t_1^2}{2D_1}\right]\tau_{xz}^{\alpha}. \tag{8}$$

Equation (8) is the governing equation for the shear strain in the adhesive.

The adhesive peel stress, σ_{zz}^{α}, is determined from a beam on elastic foundation model by considering the two adherends as beams connected by a deformable interface. The relative transverse displacements, $\tilde{w}$, of the adherends are obtained as [12]:

$$\frac{\partial^4 \tilde{w}}{\partial x^4} = -\left(\frac{1}{D_1} + \frac{1}{D_2}\right)\sigma_{zz}^{\alpha}, \tag{9}$$

where σ_{zz}^{α} is the adhesive peel stress. Equation (9) can be written as a function of adhesive peel strain, $\varepsilon_{zz}^{\alpha}$, *via* the following relationship [11]:

$$\varepsilon_{zz}^{\alpha} = \frac{1}{t_{\alpha}}(w_1 - w_2) = \frac{\tilde{w}}{t_{\alpha}}. \tag{10}$$

Substituting Eq. (10) into Eq. (9) yields:

$$\frac{\partial^4 \varepsilon_{zz}^{\alpha}}{\partial x^4} = -\frac{1}{t_{\alpha}}\left(\frac{1}{D_1}+\frac{1}{D_2}\right)\sigma_{zz}^{\alpha}. \tag{11}$$

For symmetric joints, Eq. (11) is further simplified to the following form [11]:

$$\frac{\partial^4 \varepsilon_{zz}^{\alpha}}{\partial x^4} = -\frac{2}{t_{\alpha} D_1}\sigma_{zz}^{\alpha}. \tag{12}$$

Equation (12) is the governing equation of the peel strain in the adhesive.

Note that the adhesive peel strain ($\varepsilon_{zz}^{\alpha}$) and the adhesive shear strain (γ_{xz}^{α}) are computed from the relative displacements of the adherends [see Eqs. (5) and (10)]. These quantities can be considered as the nominal (or averaged) values of the peel and shear strains through the adhesive thickness direction.

3.2. Adhesive Behavior

The constitutive behavior of the adhesive in the elastic region is given in Eq. (13) [11]. E_{α} is the Young's modulus, ν is Poisson's ratio, and G_{α} is the shear modulus of the adhesive layer.

All stresses and strains with the superscript α are the adhesive stresses and strains:

$$\begin{Bmatrix} \sigma_{xx}^{\alpha} \\ \sigma_{yy}^{\alpha} \\ \sigma_{zz}^{\alpha} \\ \tau_{yz}^{\alpha} \\ \tau_{xz}^{\alpha} \\ \tau_{xy}^{\alpha} \end{Bmatrix} = \begin{Bmatrix} 0 \\ \frac{\nu E_{\alpha}}{(1-\nu^2)}\varepsilon_{zz}^{\alpha} \\ \frac{E_{\alpha}}{(1-\nu^2)}\varepsilon_{zz}^{\alpha} \\ 0 \\ G_{\alpha}\gamma_{xz}^{\alpha} \\ 0 \end{Bmatrix}. \tag{13}$$

Generally, the adhesive normal stress, σ_{xx}^{α}, is very small compared with other adhesive stress components; hence, this stress component is assumed to be negligible [11]. Note that $\varepsilon_{xx}^{\alpha}$ is not zero in Eq. (13) and can be related to the adhesive peel strain, $\varepsilon_{zz}^{\alpha}$, *via* the plane strain assumption:

$$\varepsilon_{xx}^{\alpha} = -\frac{\nu}{1-\nu}\varepsilon_{zz}^{\alpha}. \tag{14}$$

Therefore, the two remaining independent strain components appearing in Eq. (13) are the adhesive shear strain, γ_{xz}^{α}, and the adhesive peel strain, $\varepsilon_{zz}^{\alpha}$.

3.3. Elastic Stress Solution

The governing Eqs. (8) and (12) are written in terms of adhesive peel and shear strain components ($\varepsilon_{zz}^{\alpha}$ and γ_{xz}^{α}) using the elastic constitutive relationships in Eq. (13):

$$\frac{\partial^4 \varepsilon_{zz}^{\alpha}}{\partial x^4} = -\frac{2E_{\alpha}}{D_1 t_{\alpha}(1-\nu^2)}\varepsilon_{zz}^{\alpha} \tag{15}$$

$$\frac{d^2\gamma_{xz}^{\alpha}}{dx^2} = \frac{G_{\alpha}}{t_{\alpha}}\left[\frac{2}{E_1 t_1} + \frac{t_1^2}{2D_1}\right]\gamma_{xz}^{\alpha}. \tag{16}$$

Equations (15) and (16) are solved for the adhesive peel strain, $\varepsilon_{zz}^{\alpha}$, and adhesive shear strain, γ_{xz}^{α}, respectively, as follows [11]:

$$\varepsilon_{zz}^{\alpha}(x) = C_1 \cos\beta x \cosh\beta x + C_2 \sin\beta x \sinh\beta x \tag{17}$$

$$\gamma_{xz}^{\alpha}(x) = 2C_3 \cosh\lambda x, \tag{18}$$

where

$$\beta = \frac{1}{\sqrt{2}}\left[\frac{2E_{\alpha}}{D_1 t_{\alpha}(1-\nu^2)}\right]^{1/4} \tag{19}$$

and

$$\lambda = \left[\frac{G_{\alpha}}{t_{\alpha}}\left(\frac{2}{E_1 t_1} + \frac{t_1^2}{2D_1}\right)\right]^{1/2}. \tag{20}$$

Note that Eqs. (17) and (18) account for the solutions being symmetric about $x = 0$. C_1, C_2, and C_3 in Eqs. (17) and (18) are constants and can be obtained from the boundary conditions at the right end of adherend 1 at $x = c$ (obtained in Section 3 by Eq. (10) for peel strain, $\varepsilon_{zz}^{\alpha}$):

$$\left.\frac{d^2\varepsilon_{zz}^{\alpha}}{dx^2}\right|_{x=c} = \frac{M_1(c)}{D_1 t_{\alpha}} \tag{21}$$

$$\left.\frac{d^3\varepsilon_{zz}^{\alpha}}{dx^3}\right|_{x=c} = \frac{Q_1(c)}{D_1 t_{\alpha}} \tag{22}$$

and by Eq. (6) for shear strain, γ_{xz}^{α}:

$$\left.\frac{d\gamma_{xz}^{\alpha}}{dx}\right|_{x=c} = \frac{2M_1(c)}{t_1 t_{\alpha}}\left(\frac{1}{E_1 t_1} + \frac{t_1^2}{4D_1}\right). \tag{23}$$

The above boundary conditions are applied to Eqs. (17) and (18) using Eqs. (3) and (4) to determine C_1, C_2, and C_3:

$$C_1 = \frac{M_1(c)[\cos\beta c \sinh\beta c - \sin\beta c \cosh\beta c] - Q_1(c)[\cos\beta c \cosh\beta c]}{D_1 t_\alpha \beta^3 [\sin 2\beta c + \sinh 2\beta c]} \quad (24)$$

$$C_2 = \frac{M_1(c)[\cos\beta c \sinh\beta c + \sin\beta c \cosh\beta c] - Q_1(c)[\sin\beta c \sinh\beta c]}{D_1 t_\alpha \beta^3 [\sin 2\beta c + \sinh 2\beta c]} \quad (25)$$

$$C_3 = \frac{M_1(c)}{\lambda t_\alpha t_1 \sinh\lambda c}\left(\frac{1}{E_1 t_1} + \frac{t_1^2}{4D_1}\right). \quad (26)$$

Therefore, the adhesive peel and shear stress elastic solutions are written as [11]:

$$\sigma_{zz}^{\alpha}(x) = \frac{E_\alpha}{(1-\nu^2)}(C_1 \cos\beta x \cosh\beta x + C_2 \sin\beta x \sinh\beta x) \quad (27)$$

$$\tau_{xz}^{\alpha}(x) = 2C_3 G_\alpha \cosh\lambda x. \quad (28)$$

Using Eqs. (24)–(26) and substituting in Eqs. (27) and (28), the elastic adhesive stresses are obtained and are valid within the domain of $-c \le x \le c$.

4. RESULTS AND DISCUSSION

4.1. Verification of the Model

In order to check the validity of the results of the present analysis, they are compared with those obtained in [9] in Figs. 5 and 6. Reference [9] used the first order shear deformation theory to model and analyze the smart single lap joint. However, the present analysis was on the basis of the shear lag assumption for shear stresses and on the basis of the beam on elastic foundation (BOEF) approach for the adhesive peel stress. Here, two types of piezoelectric patches are discussed: one is the common piezoelectric patch with a fully covered single-polar electrode, and the other one is a bimorph piezoelectric patch with a partly covered bipolar electrode [9]. The following material properties and geometry parameters are used for the adherends, adhesive, and piezoelectric ceramics [9]—

$$\text{Adherends: } E_1 = E_2 = 7.5 \times 10^{10}\,\text{N/m}^2, \quad \nu_1 = \nu_2 = 0.25$$

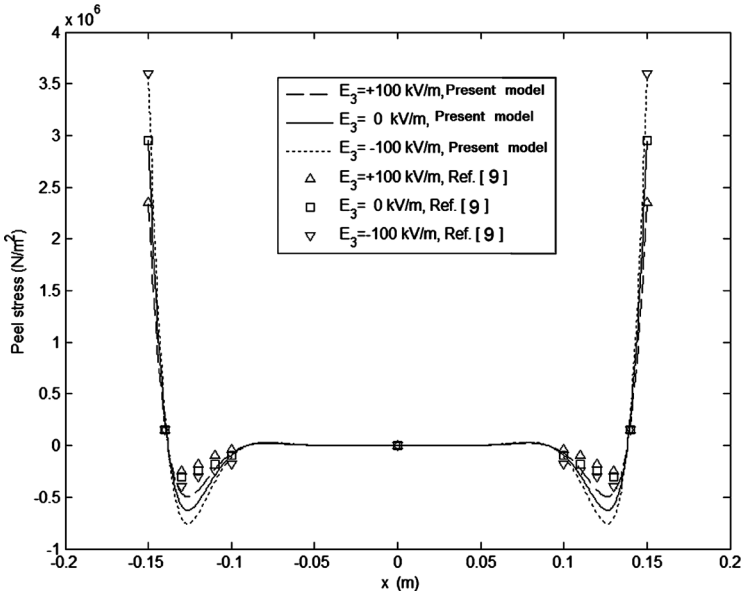

FIGURE 5 Influence of applied electric field of piezoelectric patches (with bipolar electrodes) on the peel stress in the adhesive layer. Mechanical load, $p = 37500\,\mathrm{N}$.

$$\text{Adhesive: } E_\alpha = 7.5 \times 10^9\,\mathrm{N/m^2}, \quad \nu_\alpha = 0.33$$

$$\text{Piezoelectric: } E_p = 8.4 \times 10^{10}\,\mathrm{N/m^2},\ \nu_3 = 0.22,\ d_{31} = -310 \times 10^{12}\mathrm{m/V},$$
$$l_1 = 0.5\,\mathrm{m},\ l_2 = 0.5\,\mathrm{m},\ 2l = 0.3\,\mathrm{m},\ h_\alpha = 0.5\,\mathrm{mm}.$$

Also, the thicknesses of both adherends are set to be 40 mm and the piezoelectric layer is taken as 1 mm. The mechanical load p, applied to the joint is 37500 N.

Figures 5 and 6 represent the effect of the applied electric field of bimorph piezoelectric patches having a constant length, and zero distance from the joint edge, on the peel and shear stresses of the adhesive layer. It can be seen that the maximum peel and shear stresses in the joint edges can be reduced by increasing the applied positive electric field, while the applied negative electric field can conversely increase the maximum peel and shear stresses. The maximum difference between the present analysis and Ref [9]. is less than 10% for both peel and shear stresses. This discrepancy for peel stress is near the edges and for shear stress is at the edges.

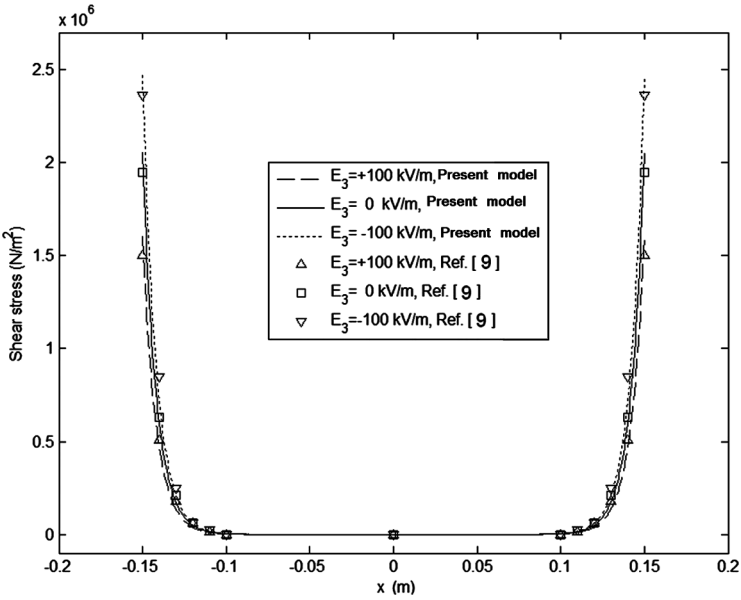

FIGURE 6 Influence of applied electric field of piezoelectric patches (with bipolar electrodes) on the shear stress in the adhesive layer. Mechanical load, $p = 37500\,\mathrm{N}$.

4.2. Adhesive Joint with Piezoelectric Patches of Bipolar Electrodes

4.2.1. Effect of Patch Electric Field

Figures 7 and 8 show the influence of the applied electric field of piezoelectric patches with bipolar electrodes on the peel and shear stresses in the adhesive layer [the patch length (2 cm) and location (0 cm from the joint edges) is fixed]. The mechanical load was $p = 37500\,\mathrm{N}$ for all the cases. By increasing the applied electric field (from -400 to $400\,\mathrm{kV/m}$):

- The peel and shear stresses in the joint edges are reduced by about 87%.
- The region of zero peel and shear stresses in the adhesive layer is wider.
- Variations of peel and shear stresses with the electric field along the overlap length are linear.
- In the case of peel stress, the rate of decrease (slope) of negative (compressive) stress is less than the rate of decrease (slope) of positive (tensile) stress as the applied electric field increases.

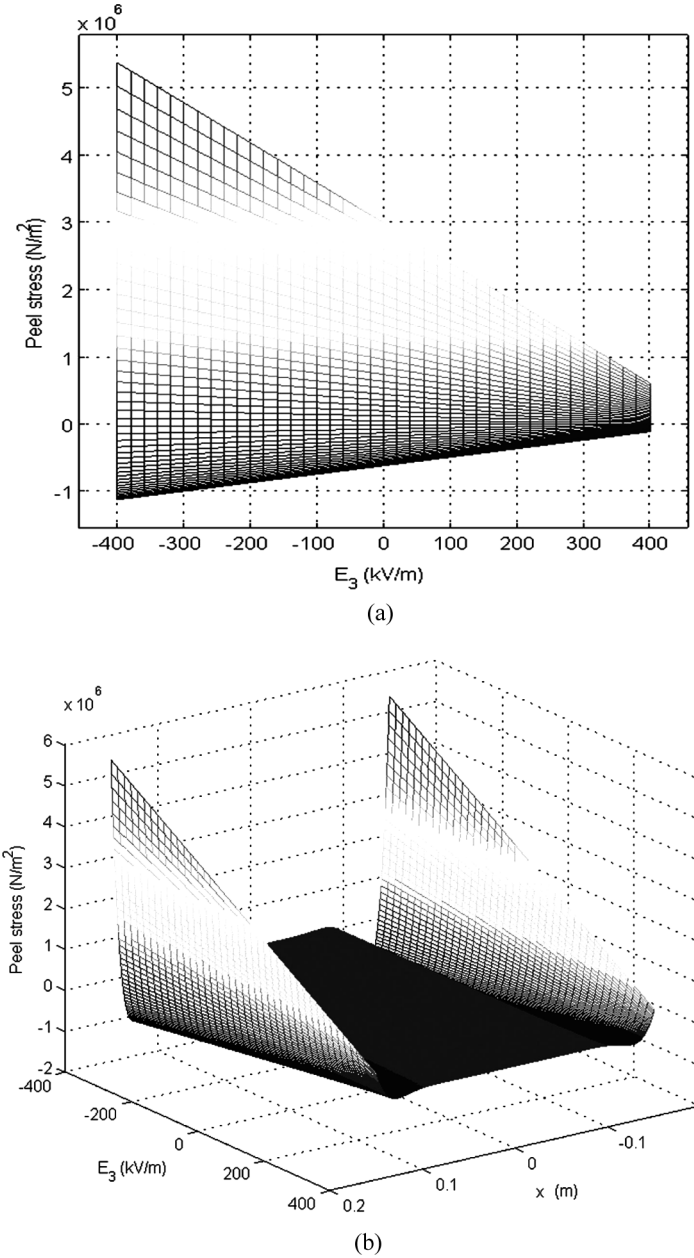

FIGURE 7 Influence of the applied electric field of piezoelectric patches (bipolar electrodes) on the peel stress in the adhesive layer. Mechanical load, $p = 37500\,\text{N}$; (a) left view, (b) isometric view.

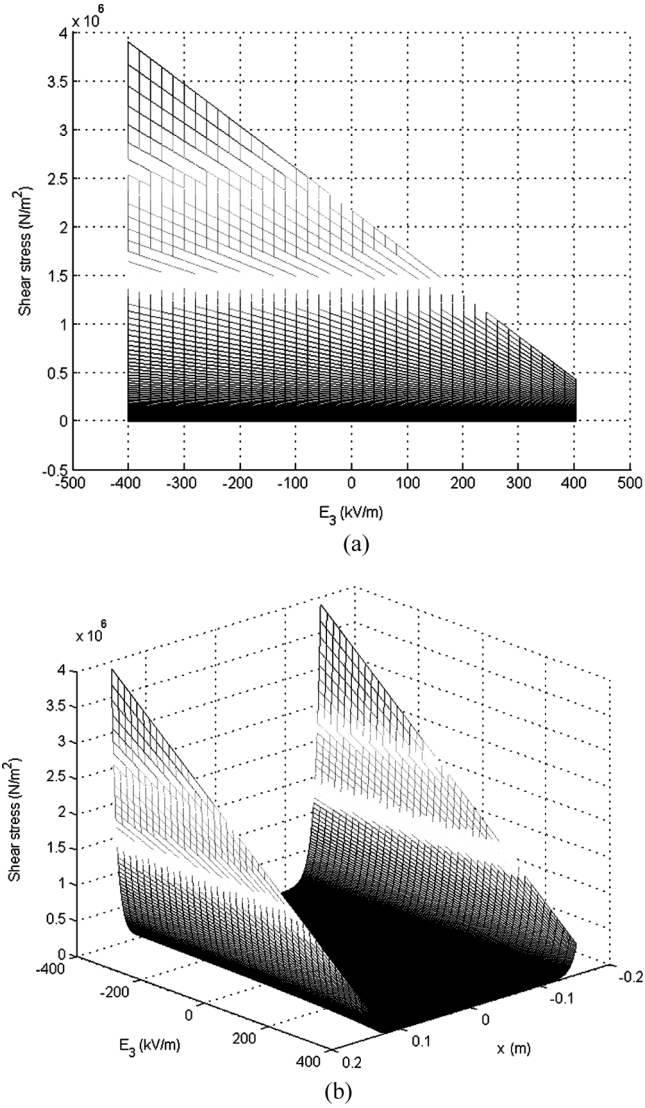

FIGURE 8 Influence of the applied electric field of piezoelectric patches (bipolar electrodes) on the shear stress in the adhesive layer. Mechanical load, $p = 37500\,\mathrm{N}$; (a) left view, (b) isometric view.

4.2.2. Effect of Patch Length

The size effect of the bonded piezoelectric patches with bipolar electrodes, in terms of length of the patch, on the peel and shear stresses is

shown in Figs. 9 and 10, respectively. These figures reveal that by increasing the length of the patches at a constant electric field (100 kV/m) and a fixed location (0 cm from the joint edges), the peel

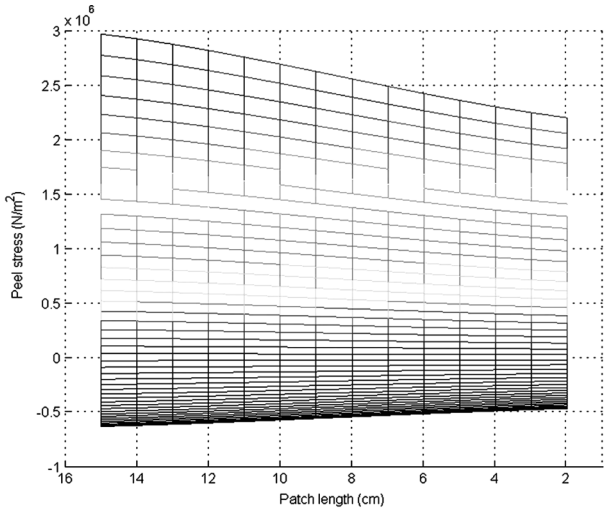

(a)

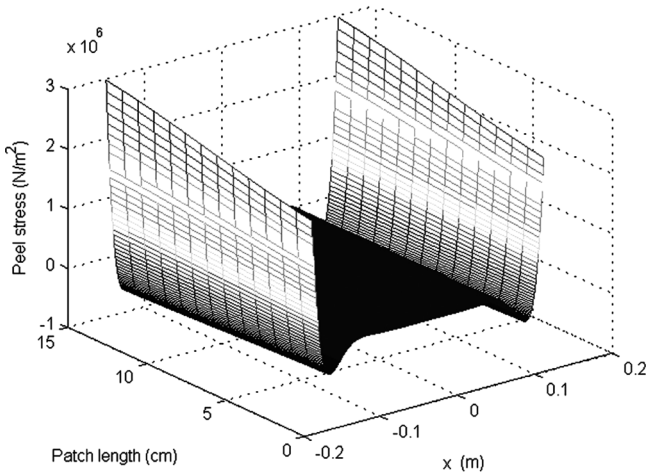

(b)

FIGURE 9 Effect of the patch length of the surface bonded piezoelectric patches (bipolar electrodes) subjected to a constant electric field ($E_3 =$ 100 kV/m) and a fixed location (0 cm from the joint edges) on the peel stress; (a) left view, (b) isometric view.

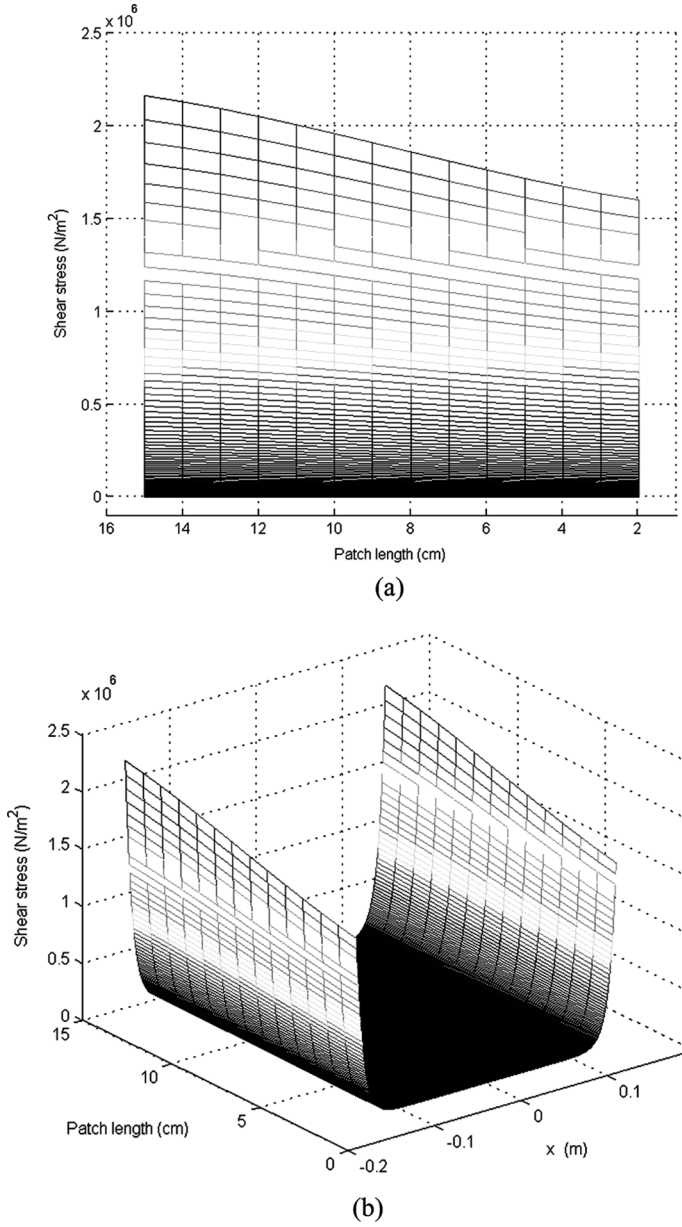

FIGURE 10 Effect of patch length of the surface bonded piezoelectric patches (bipolar electrodes) subjected to a constant electric field ($E_3 = 100\,kV/m$) and a fixed location (0 cm from the joint edges) on the shear stress; (a) left view, (b) isometric view.

and shear stresses in the joint edges are increased (by about 36%). Also, in the peel stress, the rate of increase (slope) of negative (compressive) stress is much smaller than the rate of increase (slope) of positive (tensile) stress. By increasing the patch length, the variation of positive (tensile) peel stress as well as that of the shear stress are nonlinear. However, by increasing the patch length, the variation of negative (compressive) peel stress is almost linear.

4.2.3. Effect of Patch Location

Figures 11 and 12 show the influence of the bonding location of the piezoelectric patches with bipolar electrodes [maintaining a constant electric field (100 kV/m) and a fixed length (2 cm)] on the peel and shear stresses, respectively. From these figures, it can be concluded that the change of location of the patches does not have any effect on the peel and shear stresses.

4.3. Piezoelectric Patches with Single-Polar Electrodes

The same analysis as that presented above was done to investigate the effect of single-polar piezoelectric patches on adhesive joints. Figures 13 and 14 represent the influence of the applied electric field of the piezoelectric patches with single-polar electrodes on peel and shear stresses in the adhesive layer [the patch length (2 cm) and location (0 cm from the joint edges) is fixed]. The results obtained indicate that the maximum peel and shear stresses in the joint edges increase (about 35%) by increasing the applied electric field, unlike the case of bipolar electrodes piezo patches (see Figs. 7 and 8). It means that to reduce the peel and shear stresses in the adhesive layer, a negative electric field must be applied to single-polar electrode piezoelectric patches. Also, it can be clearly seen that the peel and shear stresses can be reduced more significantly by a bimorph piezoelectric layer than by the commonly used single-polar piezoelectric layer.

Figures 15 and 16 show the size influence of the bonded piezoelectric patches with single-polar electrodes on peel and shear stresses. According to these figures, by increasing the patch length [maintaining a constant electric field (100 kV/m) and a fixed location (0 cm from the joint edges)], the peel and shear stresses at the joint edges increase (about 25%). A similar conclusion is obtained for bipolar electrodes piezoelectric patches, but the effect is larger. Also, similar to the bipolar electrodes of the piezoelectric patches, the rate of increase (slope) of negative (compressive) stress in peel stress is less than the rate of increase (slope) of positive (tensile) stress. By increasing the patch length, the variation of positive (tensile) peel stress and that

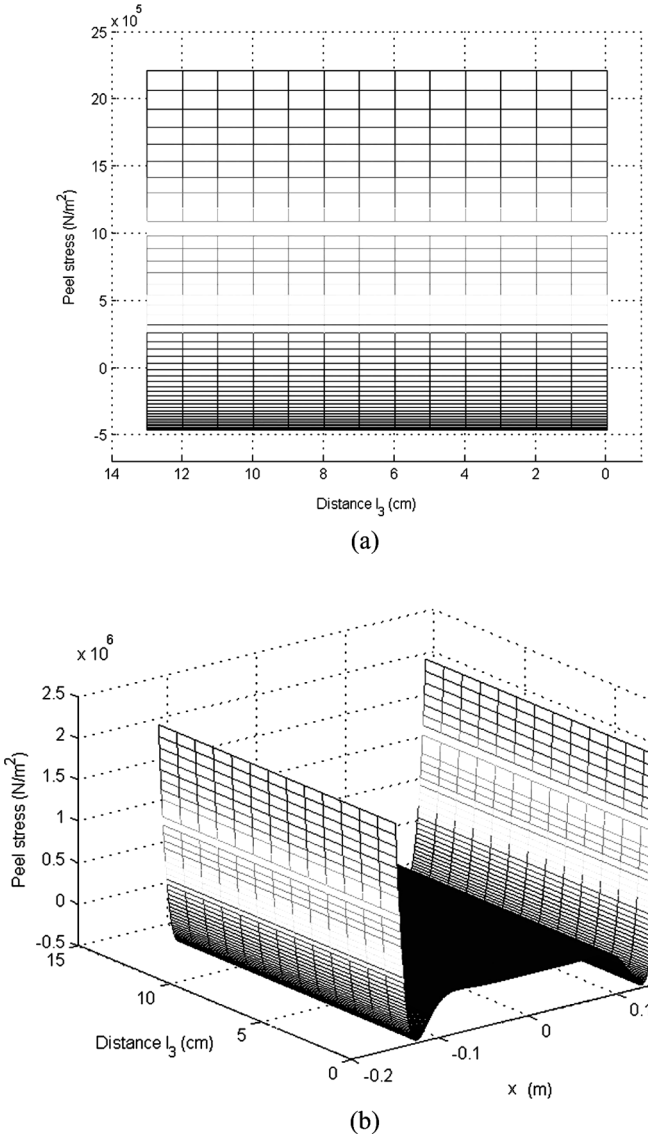

FIGURE 11 Effect of the bonding location of the surface bonded piezoelectric patches (bipolar electrodes) for a constant electric field $E_3 = 100\,\mathrm{kV/m}$ and a constant patch length (2 cm) on the peel stress; (a) left view, (b) isometric view.

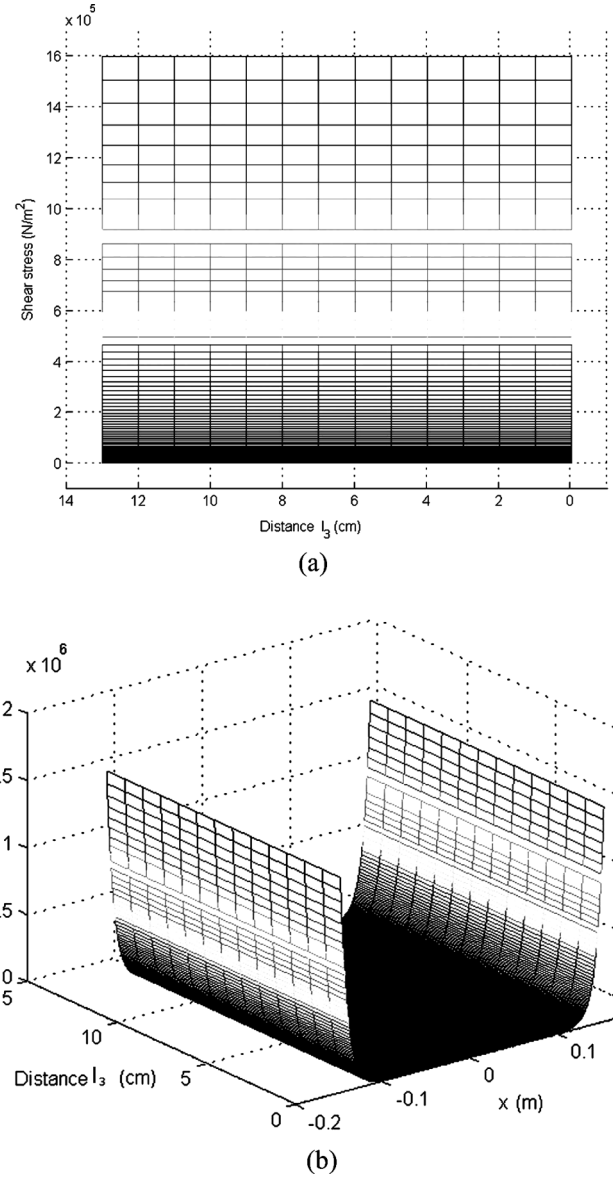

FIGURE 12 Effect of the bonding location of the surface bonded piezoelectric patches (bipolar electrodes) for a constant electric field $E_3 = 100\,kV/m$ and a constant patch length (2 cm) on the shear stress; (a) left view, (b) isometric view.

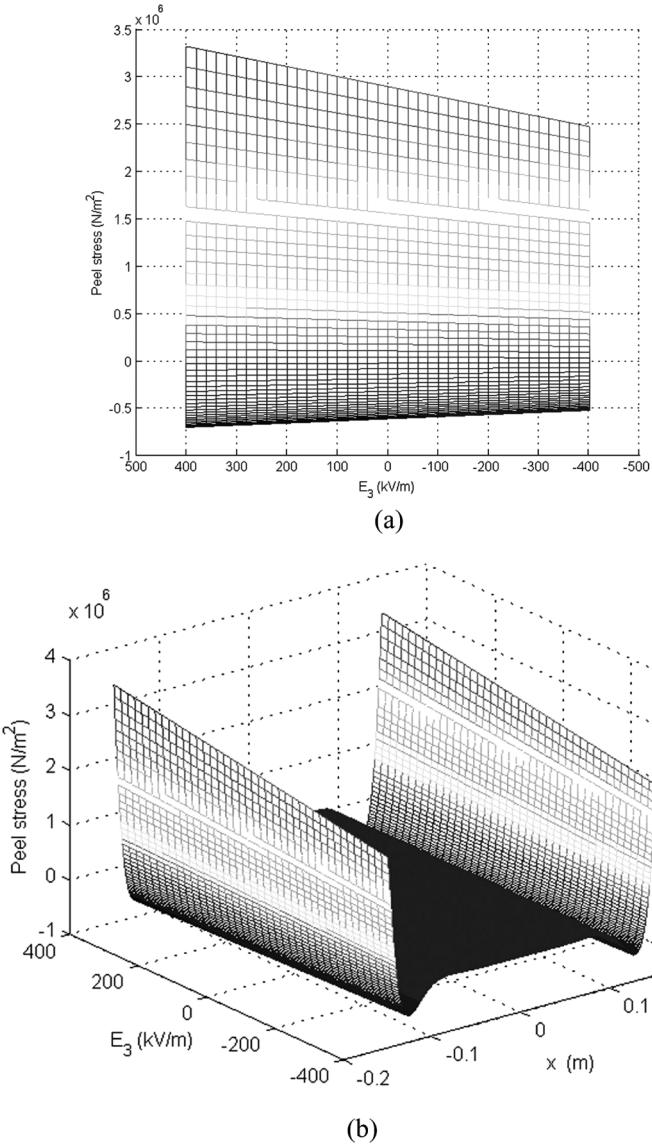

FIGURE 13 Influence of the applied electric field of piezoelectric patches (single-polar electrodes) on the peel stress in the adhesive layer. Mechanical load, $p = 37500\,\mathrm{N}$; (a) left view, (b) isometric view.

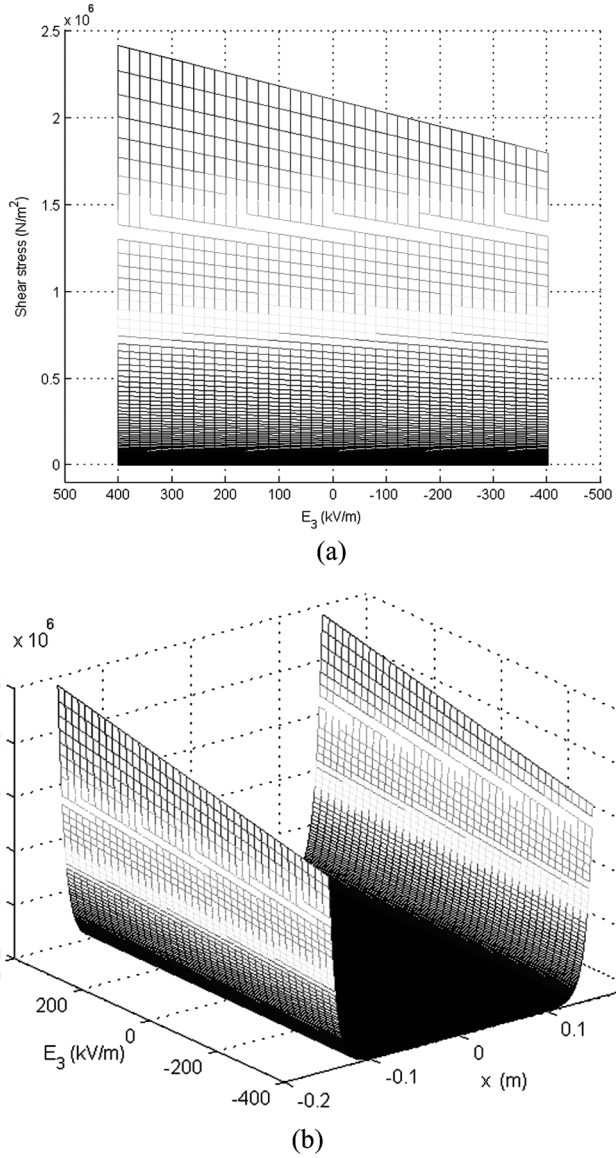

FIGURE 14 Influence of the applied electric field of piezoelectric patches (single-polar electrodes) on the shear stress in the adhesive layer. Mechanical load, $p = 37500$ N; (a) left view, (b) isometric view.

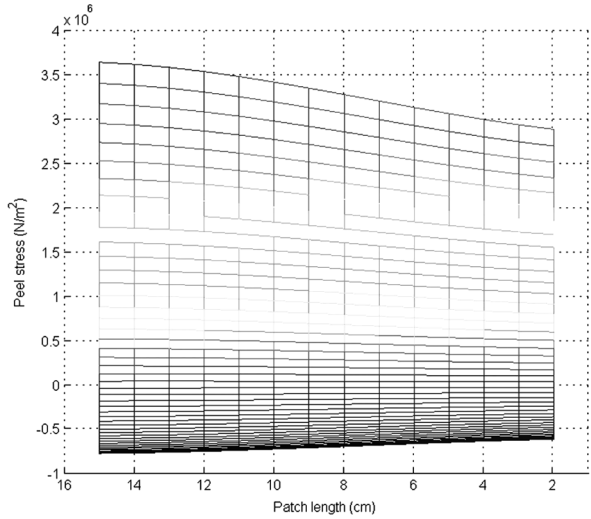

(a)

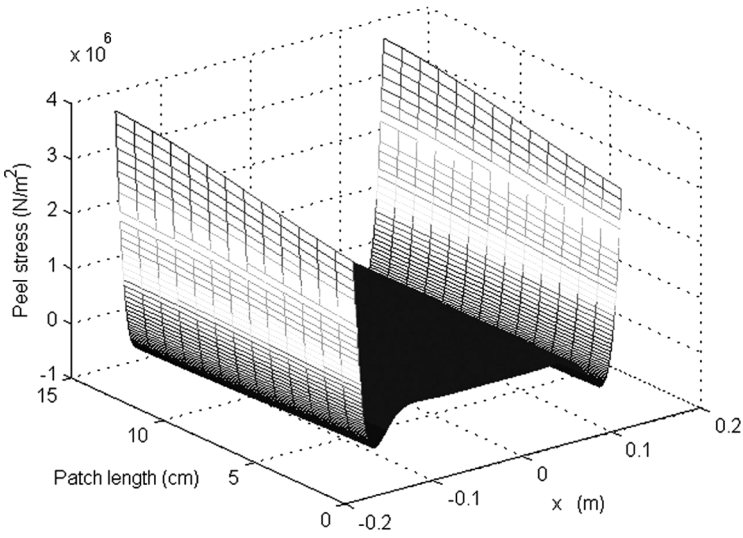

(b)

FIGURE 15 Effect of length of the surface bonded piezoelectric patches (single-polar electrodes) for a constant electric field $E_3 = 100\,kV/m$ and a fixed location (0 cm from the joint edges) on the peel stress; (a) left view, (b) isometric view.

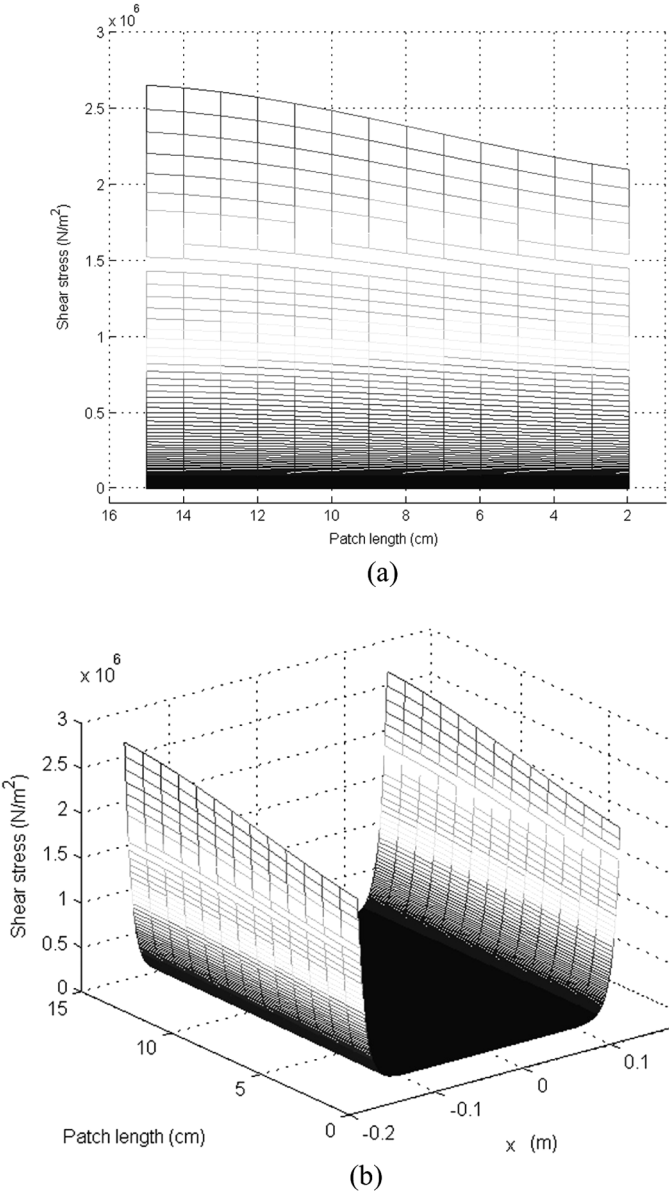

FIGURE 16 Effect of length of the surface bonded piezoelectric patches (single-polar electrodes) for a constant electric field $E_3 = 100\,kV/m$ and a fixed location (0 cm from the joint edges) on the shear stress; (a) left view, (b) isometric view.

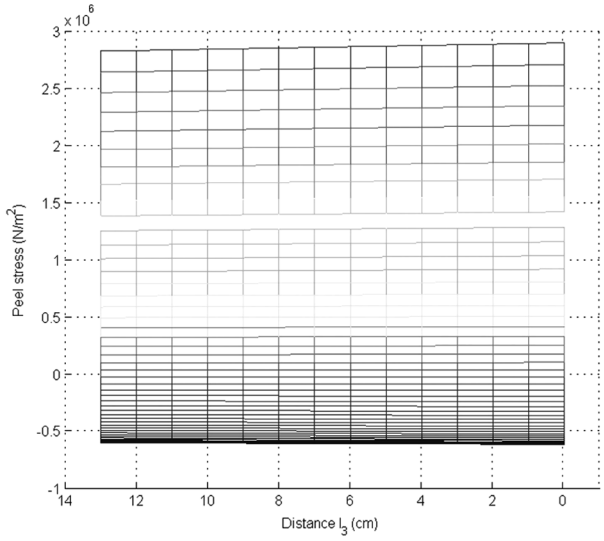

(a)

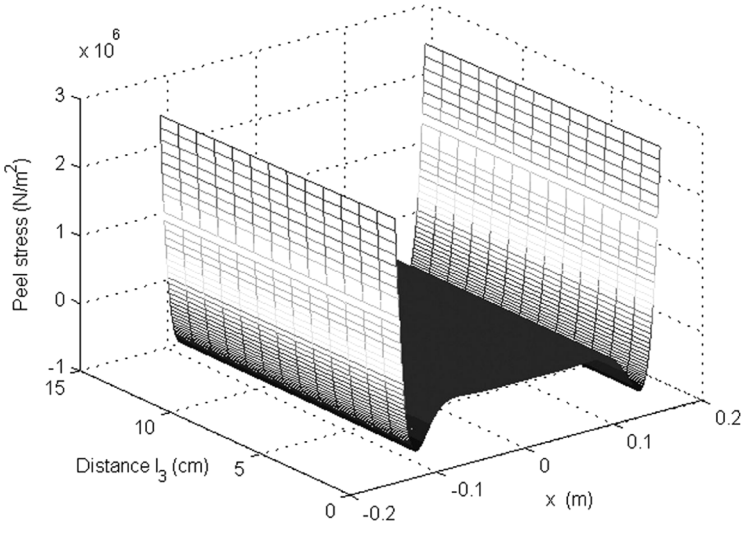

(b)

FIGURE 17 Effect of the bonding location of the surface bonded piezoelectric patches (single-polar electrodes) for a constant electric field $E_3 = 100\,kV/m$ and a constant patch length (2 cm) on the peel stress; (a) left view, (b) isometric view.

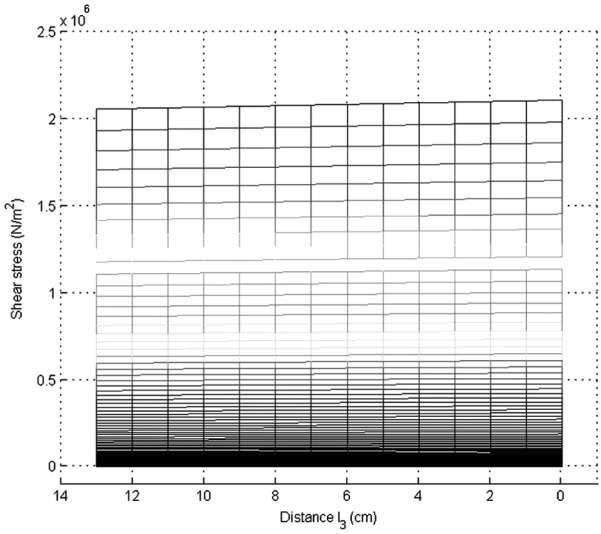

(a)

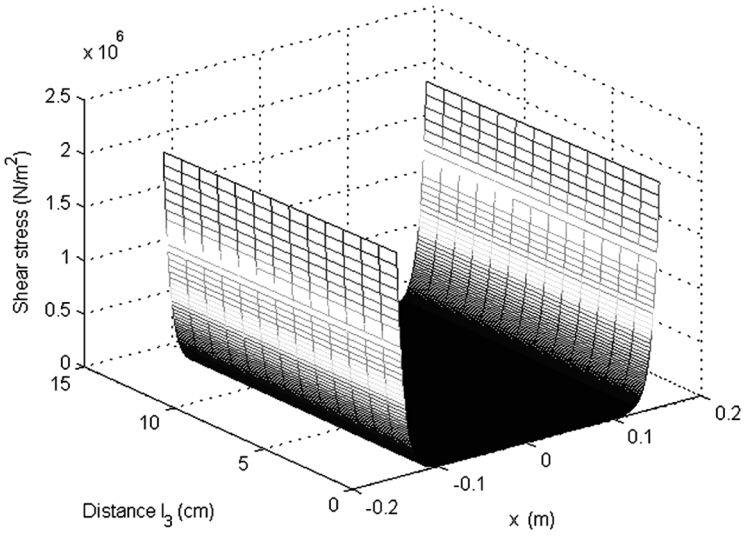

(b)

FIGURE 18 Effect of the bonding location of the surface bonded piezoelectric patches (single-polar electrodes) for a constant electric field $E_3 = 100\,kV/m$ and a constant patch length (2 cm) on the shear stress; (a) left view, (b) isometric view.

of the shear stress are nonlinear. However, by increasing the patch length, the variation of negative (compressive) peel stress is almost linear. The effect of bipolar and single-polar piezoelectric patches are almost similar.

The bonding location influence of the piezoelectric patches with single-polar electrodes on the peel and shear stresses, maintaining a constant electric field (100 kV/m) and a fixed length (2 cm) for the patches, are shown in Figs. 17 and 18. These figures show that changes in the location of the patches have only a minimal effect on peel and shear stresses of the joint. By increasing the distance from the joint edges and towards the centre of the joint, with a constant electric field and a constant patch length, the peel and shear stresses do not significantly decrease (about 4%).

5. CONCLUSIONS

Using the advantages of piezoelectric patches, a smart adhesively bonded single lap joint system was set up. In order to investigate the influence of the surface-bonded piezoelectric patches, the shear lag assumption and the beam on elastic foundation (BOEF) approach was employed to establish a detailed theoretical analytical model for evaluating the peel and shear stress distributions. Both single and bipolar piezoelectric patches were considered and the effect of electric field, patch length, and patch location from the joint edges were investigated.

It was demonstrated that by adjusting the applied electric field of the piezoelectric patches, one could adaptively control the joint-edge peel and shear stresses. Also, the results show that the peel and shear stresses change nonlinearly by increasing the patch length. However, the variation of peel and shear stresses with variation of location of the patches from the joint edges is not significant.

The present analytical model results indicate that appropriate piezoelectric patches (*i.e.,*, bimorph piezoelectric) can be used to effectively reduce the concentration of peel and shear stresses in the adhesive layer, thereby improving the performance of the joint.

REFERENCES

[1] Shiuh, C. H., *Compos. Struct.* **47**, 673–678 (1999).
[2] Goland, M. and Reissner, E., *J. Appl. Mech.* 11, A17–A27 (1944).
[3] Adams, R. D., Peppiatt, N. A., and Coppendale, J., *IEEE Trans. Nucl. Sci.* **25**, 64–78 (1978).

[4] Hart-Smith, L. J. Designing to minimize peel stresses in adhesive bonded joints in *ASTM American Society for Testing and Materials, Philadelphia, PA. STP 876*, W. S. Johnson (Ed.) (1985), pp. 238–266.
[5] Roberts, T. M. J., *J. Eng. Mech.* **115** (11), 2460–2479 (1989).
[6] Cheng, S., Chen, D., and Shi, Y. P., *J. Eng. Mech.* **117** (3), 605–623 (1991).
[7] Khalili, S. M. R., Khalili, S., Piroozhashemi, M. R., and Shokuhfar, A., *Int. J. Adhes. Adhes.* **28**, 411–428 (2008).
[8] da Silva, L. F. M. and Adams, R. D., *Int. J. Adhes. Adhes.* **27**, 227 (2007).
[9] Cheng, J. Q. and Taheri, F., *Int. J. Solids Struct.* **43** (5), 1079–1092 (2006).
[10] Cheng, J. Q. and Taheri, F., *Smart Mater. Struct.* **14** (5), 971–981 (2005).
[11] Lee, J. and Kim, H., *J. Adhesion* **83**, 837–870 (2007).
[12] Lee, J. and Kim, H., *J. Adhesion* **81** (5), 1–30 (2005).